East European Journal of Physics. 3. 589-595 (2026)
DOI:10.26565/2312-4334-2026-3-54 ISSN 2312-4334

EXPERIMENTAL CHARACTERIZATION OF SOL–GEL SPIN-COATED Al-DOPED ZnO/CdTe HETEROJUNCTION THIN FILMS

Bakhodir B. Akhmedov[1]*, Tokhirbek I. Rakhmonov[2], Mekhriddin F. Akhmadjonov[2], Sherzod Sh. Abdullayev[2], Ikhtiyor M. Tursunov[2], Fakhriddin T. Yusupov[2]
[1]*Fergana State University, Fergana, Uzbekistan*
[2]*Fergana State Technical University, Fergana, Uzbekistan*
**Corresponding author e-mail: ahmedovbahodirbahromovich@gmail.com*
Received April 11, 2026; revised July 19, 2026; accepted July 30, 2026

Al-doped zinc oxide (AZO) has attracted sustained interest as a low-cost, earth-abundant n-type transparent conducting oxide for solution-processed heterojunction photovoltaics. In the present work, undoped ZnO and AZO (2 mol% Al/Zn) thin films were deposited on p-CdTe by a sol–gel spin-coating route and examined as direct, CdS-free ZnO(AZO)/CdTe heterojunctions – a configuration for which experimental reports remain scarce. The structural, optical, electrical, and morphological responses were investigated by XRD, UV–Vis absorbance spectroscopy with first-derivative band-edge analysis, dark and illuminated J–V measurements with Cheung–Cheung diode-parameter extraction, and SEM. XRD confirmed the coexistence of zinc-blende CdTe and c-axis-oriented wurtzite ZnO, with Scherrer crystallite sizes of 27 ± 5 nm. The derivative absorbance maximum shifted from 3.31 eV (ZnO) to 3.33 eV (AZO). Under illumination, the AZO/CdTe device yielded $J_{sc} \approx 4.2\ mA \cdot cm^{-2}$, $V_{oc} \approx 0.43\ V$, with $n \approx 3.1$, $R_s \approx 28\ \Omega \cdot cm^2$, $R_{sh} \approx 310\ \Omega \cdot cm^2$, $F_F \approx 27\%$, $\eta \approx 0.49\%$. SEM revealed a pinhole-free polycrystalline AZO overlayer (30–80 nm grains). The results establish a baseline characterization of buffer-free, solution-processed AZO/CdTe heterojunctions.
Keywords: *Al-doped ZnO; CdTe heterojunction; Sol–gel spin coating; Transparent conducting oxide; Tauc plot; Ideality factor; Cheung–Cheung method; Thin-film photovoltaics*

INTRODUCTION

Transparent conducting oxides (TCOs) constitute a critical functional layer in thin-film heterojunction photovoltaic devices, where they must simultaneously provide high optical transparency, adequate electrical conductivity, and chemical compatibility with the underlying absorber [1]. Among the available TCO candidates, Al-doped zinc oxide (AZO) has emerged as a particularly attractive alternative to indium-based oxides owing to the natural abundance of its constituent elements, the chemical and thermal stability of the ZnO host lattice, and the strong tunability of its optoelectronic properties through Al incorporation [2,3]. Recent comprehensive reviews have confirmed that solution-processed AZO can achieve carrier concentrations in the $10^{20} - 10^{21}\ cm^{-3}$ range while maintaining optical transmittance above 80% [4,5].

Sol–gel spin coating offers a low-cost and compositionally flexible deposition route well suited to research-scale investigation of doped oxide films. Rahman et al. demonstrated that sol–gel spin-coated AZO films can exhibit transmittance values approaching 96% with crystallite sizes of approximately 20 nm [6], while Khan et al. reported enhanced optoelectronic response after UV irradiation [7]. Systematic studies have shown that Al concentration strongly influences crystallite size, texture, and near-edge optical behavior [8–10]. A shift of the optical edge toward higher photon energies is commonly interpreted as a Burstein–Moss effect, although disorder-related band-tail formation can contribute simultaneously.

CdTe remains one of the leading thin-film photovoltaic materials, with record laboratory efficiencies exceeding 22% and cumulative installed capacity above 30 GWp [11,12]. The majority of commercial CdTe devices employ a CdS buffer layer between the TCO window and the CdTe absorber [11,13]. However, CdS introduces parasitic absorption losses in the blue spectral region and adds environmental concerns. Direct ZnO-based window layers deposited onto CdTe represent a structurally simpler alternative. Early work demonstrated that n-ZnO/p-CdTe junctions can exhibit clear rectifying behavior without a CdS buffer [14], and recent SCAPS-1D simulations by Zepeda Medina et al. predicted AZO/CdTe heterostructures capable of PCE above 14% [15,16]. A closely related investigation published in this journal confirmed the feasibility of Al-doped ZnO heterostructures on silicon [17]. Nevertheless, experimental reports of direct AZO/CdTe heterojunctions without an intervening CdS buffer layer remain extremely scarce in the open literature [15]. The present work addresses this gap by providing a coherent experimental characterization of sol–gel spin-coated AZO/CdTe heterojunctions prepared without a CdS buffer layer. The approach combines XRD with Scherrer crystallite-size analysis, UV–Vis absorbance with derivative and Tauc-plot bandgap extraction, dark and illuminated J–V measurements with quantitative Cheung–Cheung diode-parameter extraction, and SEM. A quantitative comparison with prior ZnO/CdTe and AZO/CdTe devices is also provided. A schematic of the heterojunction is shown in Figure 1.

Cite as: B.B. Akhmedov, T.I. Rakhmonov, M.F. Akhmadjonov, Sh.Sh. Abdullayev, I.M. Tursunov, F.T. Yusupov, East Eur. J. Phys. 3, 589 (2026), https://doi.org/10.26565/2312-4334-2026-3-54

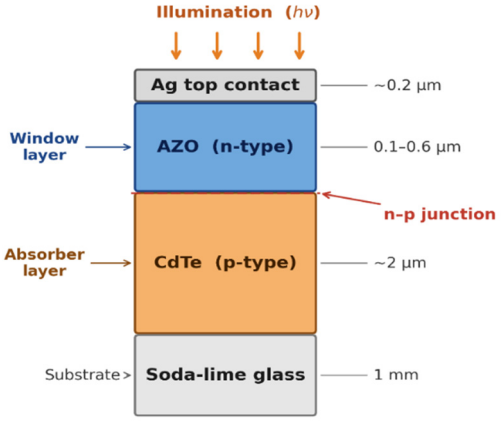

Figure 1. Schematic cross-section of the AZO/CdTe heterojunction structure investigated in this work

EXPERIMENTAL DETAILS

Materials and substrate preparation. Zinc acetate dihydrate [$Zn(CH_3COO)_2 \cdot 2H_2O$, ≥99.0%, Sigma-Aldrich] was used as the zinc precursor, aluminum nitrate nonahydrate [$Al(NO_3)_3 \cdot 9H_2O$, ≥98.0%, Sigma-Aldrich] as the Al dopant source, monoethanolamine [MEA, ≥99.5%, Sigma-Aldrich] as the stabilizing and complexing agent, and absolute ethanol (≥99.8%) as the solvent. p-type polycrystalline CdTe layers on soda-lime glass served as the substrates. Prior to deposition, the CdTe substrates were sequentially cleaned by ultrasonication in acetone (10 min), isopropanol (10 min), and deionized water (10 min), then dried under high-purity nitrogen.

Sol preparation. The ZnO precursor sol was prepared by dissolving zinc acetate dihydrate in absolute ethanol to yield a Zn^{2+} concentration of 0.60 mol L^{-1}. For Al-doped sols, aluminum nitrate nonahydrate was added to give an Al/Zn molar ratio of 2 mol%, selected based on previous optimization studies [6,8,10]. Monoethanolamine was introduced at an equimolar ratio (Zn:MEA = 1:1). The mixture was stirred at 65 °C for 60 min until a clear homogeneous sol was obtained, then aged at 24 ± 2 °C for 24 h. The sol was filtered through a 0.22 μm PTFE syringe filter.

Thin-film deposition. Films were deposited by a two-step spin-coating sequence: initial spreading at 500 rpm for 10 s followed by thinning at 3000 rpm for 30 s. Approximately 0.2 mL of filtered sol was dispensed onto each substrate. After each coating cycle, intermediate drying/pyrolysis was performed at 250 °C for 10 min in air. The coating/pyrolysis sequence was repeated 10 times. Following the final cycle, films were annealed at 500 °C for 45 min in air with heating and cooling rates of ~5 °C min^{-1}. Final overlayer thickness was in the 0.10–0.60 μm range, as determined by cross-sectional SEM.

Characterization techniques. X-ray diffraction (XRD) was performed using Cu Kα radiation (λ = 0.15406 nm) at 40 kV and 30 mA in the 2θ range of 20°–60° with a step size of 0.02° and scan rate of 2° min^{-1}. Peak identification used JCPDS PDF 15-0770 (CdTe) and PDF 36-1451 (ZnO). Average crystallite size was estimated from the Scherrer equation:

$$D = \frac{K\lambda}{\beta \cos\theta}, \tag{1}$$

where K = 0.9, β is the FWHM corrected for instrumental broadening, and θ is the Bragg angle. UV–Vis absorbance was recorded with a double-beam spectrophotometer over 200–800 nm. Optical bandgap was extracted via the Tauc relation for direct allowed transitions:

$$(\alpha h\nu)^2 = B(h\nu - E_g), \tag{2}$$

where $\alpha = 2.303A/t$. J–V measurements used a source–measure unit over −0.5 to +0.8 V with 10 mV step, under dark and ~100 mW cm^{-2} illumination. The active area was 0.25 cm^2, with silver-paste contacts.

Diode parameters (n, Rs) were extracted via the Cheung–Cheung method:

$$\frac{dV}{d(\ln J)} = R_s \cdot J + n\left(\frac{kT}{q}\right). \tag{3}$$

Shunt resistance was obtained from $R_{sh} = \left.\frac{dV}{dJ}\right|_{V\to 0}$. SEM was operated at 15 kV; the average grain size was determined from at least 50 grains.

RESULTS AND DISCUSSION

Structural properties. Figure 2 shows the XRD pattern of the AZO/CdTe heterojunction. Reflections from both zinc-blende CdTe and wurtzite ZnO are clearly resolved. The most intense reflection at $2\theta \approx 23.8°$ is indexed to CdTe (111), indicating pronounced ⟨111⟩ preferred orientation [11,12]. Additional CdTe reflections at 39.3°, 46.5°, and 56.8° correspond to (220), (311), and (400) planes (JCPDS PDF 15-0770). The wurtzite ZnO overlayer contributes reflections at 31.8°, 34.4°, and 36.3°, indexed to (100), (002), and (101) of hexagonal ZnO (JCPDS PDF 36-1451). The (002)

reflection is the most intense, indicating c-axis preferred orientation, a well-known feature of sol–gel AZO films attributed to surface-free-energy minimization [6,8].

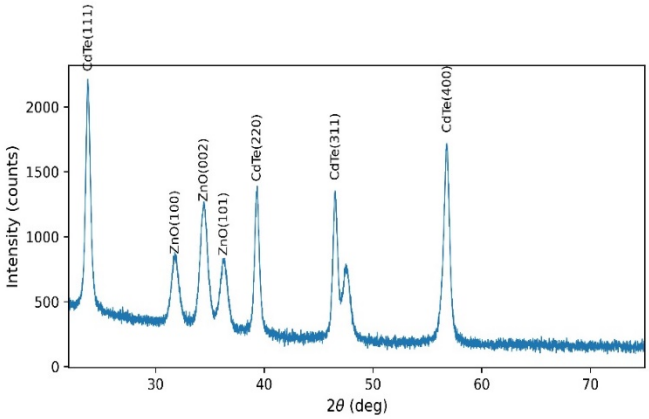

Figure 2. XRD pattern of the AZO/CdTe heterojunction showing coexistence of zinc-blende CdTe and wurtzite ZnO

The Scherrer equation (Eq. 1), applied to the dominant ZnO (002) peak with FWHM ≈ 0.38° yields D(002) ≈ 22 nm. The same analysis of the (100) and (101) peaks yields 25–35 nm, with an average of 27 ± 5 nm for the AZO overlayer. These values agree with sol–gel spin-coated AZO films annealed at 450–550 °C [6,9,10]. For CdTe (111), the calculated crystallite size is ~45 nm. The absence of Al- or Al_2O_3-related reflections suggests that Al is either incorporated into the ZnO lattice or dispersed below the XRD detection limit [8,9].

Optical properties. Figure 3 compares the optical absorbance spectra of undoped ZnO and AZO films. Both films exhibit strong UV absorbance below ~380 nm, followed by a sharp decrease at longer wavelengths. The undoped ZnO film exhibits a steep absorption edge in the 360–380 nm range. The AZO film exhibits systematically higher absorbance across the entire range, with a broader near-edge region and an enhanced baseline at longer wavelengths, attributable to free-carrier absorption and disorder-related sub-band-edge states [7,8].

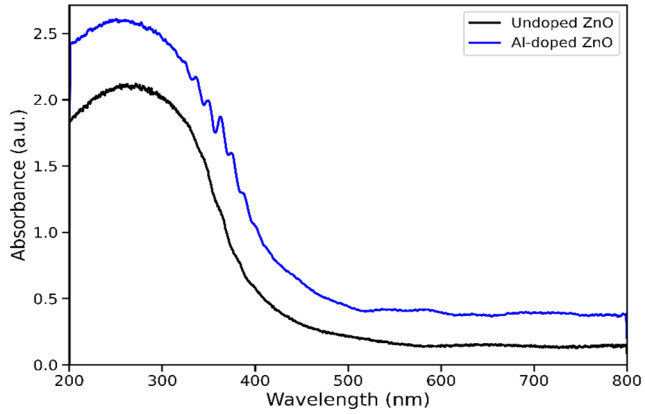

Figure 3. UV–Vis absorbance spectra of undoped ZnO and AZO thin films

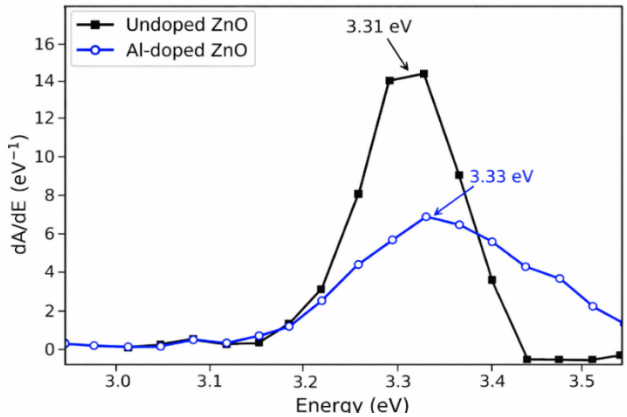

Figure 4. First-derivative absorbance dA/dE of undoped ZnO and AZO films, revealing the band-edge shift from 3.31 eV to 3.33 eV

The first derivative dA/dE is shown in Figure 4. The undoped ZnO film exhibits a sharp derivative maximum at 3.31 ± 0.01 eV (FWHM ≈ 0.09 eV), while the AZO film shows a broader feature at 3.33 ± 0.01 eV with an extended

high-energy tail up to ~3.45 eV. The derivative analysis therefore reveals (i) a reproducible blue shift of ΔE ≈ 0.02 eV and (ii) pronounced broadening of the band-edge region. The blue shift is consistent with a Burstein–Moss effect from donor electrons contributed by Al^{3+} substitution [8–10], but its small magnitude (compared to heavily doped AZO [9]) and the simultaneous broadening indicate that disorder-related band-tail formation also contributes [7,8].

Figure 5 shows the Tauc plots for both films. Linear extrapolation yields Eg(ZnO) = 3.27 ± 0.02 eV and Eg(AZO) = 3.31 ± 0.02 eV, corresponding to a Tauc-based shift of ΔEg ≈ 0.04 eV. Both derivative and Tauc analyses consistently support a small blue shift of the effective bandgap upon Al incorporation, accompanied by band-edge broadening characteristic of moderately doped sol–gel AZO films.

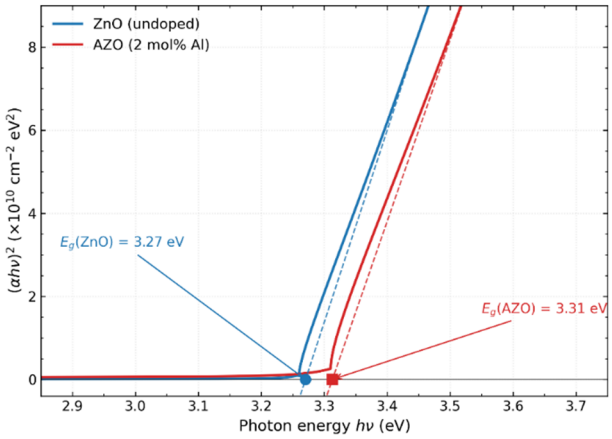

Figure 5. Tauc plot (αhν)² versus hν for undoped ZnO and AZO films, with linear extrapolations yielding Eg(ZnO) = 3.27 eV and Eg(AZO) = 3.31 eV

Surface morphology. Figure 6 shows representative plan-view and cross-sectional SEM images. The plan-view reveals a continuous polycrystalline AZO overlayer with densely packed grains of 30–80 nm and an average grain size of 52 ± 12 nm (from 50 grains). The film exhibits full lateral coverage without macroscopic voids, cracks, or pinholes. The difference between SEM grain size (~52 nm) and XRD crystallite size (~27 nm) indicates that individual grains comprise multiple coherently diffracting crystallites, common in polycrystalline sol–gel films [6,9]. The cross-sectional image confirms a continuous overlayer with a distinct AZO/CdTe interface and no macroscopic delamination.

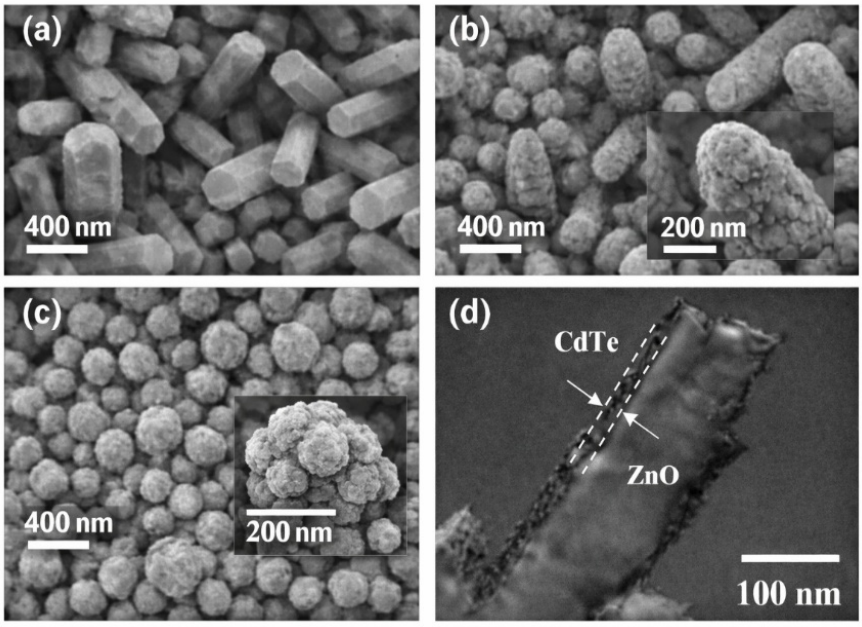

Figure 6. Plan-view and cross-sectional SEM images of the AZO/CdTe heterostructure

Electrical and photovoltaic properties. Figure 7 presents the dark and illuminated J–V characteristics. Under dark conditions, diode-like rectification is observed with a forward current onset above $\sim 0.4\,V$. Under $\sim 100\,mW \cdot cm^{-2}$ illumination, $J_{sc} = 4.2 \pm 0.2\,mA \cdot cm^{-2}$ and $V_{oc} = 0.43 \pm 0.02\,V$, yielding $F_F \approx 27\%$ and $\eta \approx 0.49\%$. These values confirm a functional photovoltaic response, while the low fill factor indicates non-idealities consistent with an unoptimized buffer-free device.

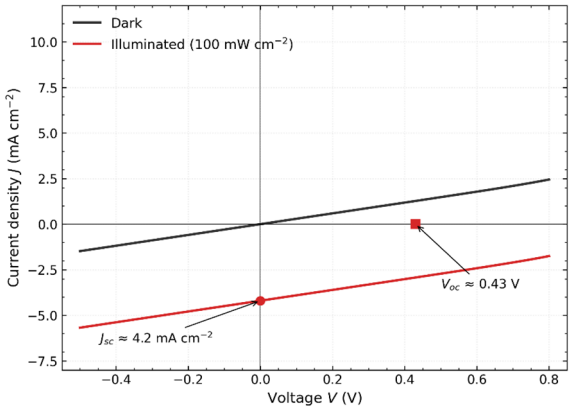

Figure 7. Dark and illuminated current density–voltage characteristics of the AZO/CdTe heterojunction.

Figure 8 shows the $dV/d(ln\,J)$ vs. J plot for the forward-bias region ($V > 0.45\,V$). Linear fitting according to Eq. (3) yields R_s and $n(kT/q)$. The extracted parameters are summarized in Table 1.

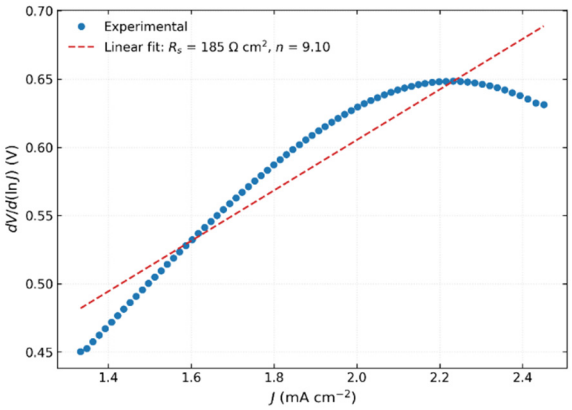

Figure 8. Cheung–Cheung plot dV/d(ln J) versus J for the AZO/CdTe heterojunction, yielding n = 3.1 and Rs = 28 Ω cm²

Table 1. Photovoltaic and diode parameters of the AZO/CdTe heterojunction

Parameter	Value	Method
$J_{sc}(mA \cdot cm^{-2})$	4.2 ± 0.2	Illuminated J–V (V = 0)
$V_{oc}\ (V)$	0.43 ± 0.02	Illuminated J–V (J = 0)
$F_F\ (\%)$	27 ± 3	Maximum power point
$\eta\ (\%)$	0.49 ± 0.05	Pmax / Pin
n	3.1 ± 0.2	Cheung–Cheung [Eq. 3]
$R_s\ (\Omega \cdot cm^2)$	28 ± 4	Cheung–Cheung [Eq. 3]
$R_{sh}\ (\Omega \cdot cm^2)$	310 ± 25	dV/dJ at $V \rightarrow 0$

The ideality factor $n \approx 3.1$ rules out pure diffusion-limited transport ($n = 1$) and exceeds the value for space-charge recombination alone ($n = 2$). Values in the range 2–5 are commonly reported for polycrystalline CdTe heterojunctions and are typically attributed to trap-assisted tunneling across interface states, grain-boundary recombination, and multi-level recombination in the depletion region [18,23]. In the present buffer-free structure, the absence of a CdS layer eliminates the conventional lattice-matched interface, thereby leaving a direct AZO/CdTe contact that is inherently more susceptible to interface-state recombination. The series resistance $R_s \approx 28\,\Omega \cdot cm^2$ is approximately an order of magnitude higher than that of optimized sputtered AZO/CdS/CdTe devices ($\sim 1 - 3\,\Omega \cdot cm^2$) [11,15], reflecting the resistive sol–gel AZO, silver-paste contacts, and – most importantly – the absence of $CdCl_2$ activation [11,13]. The moderate $R_{sh} \approx 310\,\Omega \cdot cm^2$ is consistent with the pinhole-free morphology but indicates residual grain-boundary-mediated leakage [18]. Importantly, none of these limitations is intrinsic to the AZO/CdTe concept; each is tractable through $CdCl_2$ activation, grain-boundary passivation, AZO thickness optimization, and sputtered metal contacts.

Comparative analysis. Table 2 compares the present results with previously reported ZnO/CdTe and AZO/CdTe devices. Direct experimental AZO/CdTe devices without a CdS buffer remain exceptionally rare – a point explicitly noted by Zepeda Medina et al. [15].

Table 2. Comparison of photovoltaic parameters for ZnO/CdTe and AZO/CdTe heterojunctions.

Ref.	Structure	Method	Jsc	Voc	FF	η	Type
[14]	n-ZnO/p-CdTe	Spray pyrolysis	19.5	0.54	53	8.8	Expt
[21]	AZO/i:ZnO/CdS/CdTe	Sputter+evap.	24.7	0.84	75.5	15.6	Expt
[22]	AZO/CdS/CdTe	All-sputtered	23	0.82	65	14.0	Expt
[15]	Al/AZO/CdTe/NiO/Ni	SCAPS-1D	26.2	0.74	72.8	14.2	Sim
[16]	AZO/CdTe/$FeSi_2$	SCAPS-1D	51.4	0.63	83.1	27.2	Sim
This work	AZO/CdTe (no CdS)	Sol–gel spin	4.2	0.43	27	0.49	Expt

Three observations emerge. First, all high-efficiency experimental devices [21,22] employ a CdS buffer and high-temperature sputtering/evaporation, confirming that sol–gel processing combined with a CdS-free architecture represents a distinct and less-explored configuration. Second, the present J_{sc} ($4.2\ mA \cdot cm^{-2}$) falls below both the spray-pyrolysis ZnO/CdTe result [14] and the SCAPS-1D prediction [15], indicating substantial room for improvement through $CdCl_2$ activation. Third, the present Voc (0.43 V) is lower than the simulation prediction ($0.74\ V$) by $\Delta V_{oc} \approx 0.3\ V$, quantitatively consistent with the additional Shockley–Read–Hall recombination losses $\Delta V_{oc} = n(kT/q) \cdot ln(J0, real/J0, ideal)$ expected at an unpassivated interface with n ≈ 3.1.

CONCLUSIONS

In this work, Al-doped zinc oxide (2 mol% Al/Zn) and undoped ZnO thin films were deposited on p-CdTe by a sol–gel spin-coating route to form direct, CdS-free ZnO(AZO)/CdTe heterojunctions. The structural, optical, electrical, and morphological responses were investigated through a coherent combination of XRD, UV–Vis spectroscopy with derivative and Tauc analyses, dark and illuminated J–V measurements with quantitative Cheung–Cheung diode-parameter extraction, and SEM.

XRD confirmed the coexistence of zinc-blende CdTe and c-axis-oriented wurtzite ZnO, with Scherrer crystallite sizes of 27 ± 5 nm. UV–Vis analysis revealed a small blue shift of the band-edge response upon Al incorporation – from 3.27 eV to 3.31 eV by Tauc extrapolation and from 3.31 eV to 3.33 eV by derivative analysis – supporting an interpretation involving a mild Burstein–Moss contribution superimposed on disorder-induced broadening. The AZO/CdTe heterojunction exhibited diode-like rectification and measurable photoresponse ($J_{sc} = 4.2\ mA \cdot cm^{-2}$, $V_{oc} = 0.43\ V$, $F_F \approx 27\%$, $\eta \approx 0.49\%$). Cheung–Cheung analysis yielded $n \approx 3.1$, $R_s \approx 28\ \Omega \cdot cm^2$, and $R_{sh} \approx 310\ \Omega \cdot cm^2$, providing a quantitative mechanistic explanation: the photovoltaic response is primarily limited by interface-state recombination, grain-boundary-mediated losses, and the absence of $CdCl_2$ activation – none of which are intrinsic to the AZO/CdTe concept itself. SEM revealed a continuous pinhole-free polycrystalline AZO overlayer (30–80 nm grains, 0.10–0.60 μm thick).

Taken together, these results establish one of the first experimentally characterized sol–gel spin-coated AZO/CdTe heterojunctions reported without a CdS buffer layer, providing a quantitative baseline for future optimization. Future work should focus on: (i) systematic variation of the Al doping level in the 1–4 mol% range; (ii) $CdCl_2$ activation treatment; (iii) optimization of AZO overlayer thickness and annealing profile; and (iv) replacement of silver-paste contacts with sputtered metal electrodes. Progress along these axes is expected to close the gap between the present experimental device (η ≈ 0.49%) and the SCAPS-1D prediction (η ≈ 14%) for optimized AZO/CdTe structures.

Acknowledgments

The authors gratefully acknowledge the financial and infrastructural support provided by Fergana State Technical University, Uzbekistan. The authors thank the Laboratory staff for technical assistance with XRD, UV–Vis, and SEM measurements. The authors declare no conflict of interest. Language-editing assistance was limited to grammar and style refinement; no generative AI tools were used in the formulation of scientific content.

ORCID

Bakhodir B. Akhmedov, https://orcid.org/0000-0003-4894-3588; **Tokhirbek I. Rakhmonov,** https://orcid.org/0000-0002-6080-6159; **Mekhriddin F. Akhmadjonov,** https://orcid.org/0000-0002-1623-0404; **Sherzod Sh. Abdullayev,** https://orcid.org/0009-0007-9768-5008; **Ikhtiyor M. Tursunov,** https://orcid.org/0009-0009-0864-2204; **Fakhriddin T. Yusupov,** https://orcid.org/0000-0001-8937-7944

REFERENCES

[1] G.T. Chavan, Y. Kim, M.Q. Khokhar, S.Q. Hussain, E.-C. Cho, J. Yi, Z. Ahmad, P. Rosaiah, and C.-W. Jeon, "A brief review of transparent conducting oxides (TCO)," Nanomaterials, **13**(7), 1226 (2023). https://doi.org/10.3390/nano13071226

[2] F.T. Yusupov, V.T. Mirzaev, T.I. Rakhmonov, O.R. Nurmatov, and D.Sh. Khidirov, "Enhanced optoelectronic properties of ZnO thin films through boron and fluorine co-doping," J. Ovonic Res. **21**(3), 285–296 (2025). https://doi.org/10.15251/JOR.2025.213.285

[3] M. Gartner, H. Stroescu, D. Mitrea, and M. Nicolescu, "Various applications of ZnO thin films obtained by chemical routes in the last decade," Molecules, **28**(12), 4674 (2023). https://doi.org/10.3390/molecules28124674

[4] J. Lee, *et al*., "Advancing Al-doped ZnO thin films structural, optical and electrical properties via flash lamp annealing," J. Semicond. **45**(12), 122101 (2024). https://doi.org/10.1088/1674-4926/24070005

[5] C. Djidjeli, A. Chelouche, T. Touam, and D. Djouadi, "Ag nanoparticles effects on physical properties of ZnO and AZO sol–gel thin films," J. Mater. Sci.: Mater. Electron. **34**, 1765 (2023). https://doi.org/10.1007/s10854-023-11167-2

[6] M.R. Rahman, *et al*., "Conductive and optically transparent sol–gel spin coated Al^{3+} and Sn^{4+} doped ZnO nano-crystalline thin-films," J. Mater. Sci.: Mater. Electron. **35**, 1618 (2024). https://doi.org/10.1007/s10854-024-13328-3

[7] M.I. Khan, T.R. Neha, and M.M. Billah, "UV-irradiated sol-gel spin coated AZO thin films: Enhanced optoelectronic properties," Heliyon, **8**(1), e08743 (2022). https://doi.org/10.1016/j.heliyon.2022.e08743
[8] H. Stroescu, *et al*., "Effect of Al incorporation on the structural and optical properties of sol–gel AZO thin films," Materials, **16**(9), 3329 (2023). https://doi.org/10.3390/ma16093329
[9] A.M. Al-Shehri, S. Alshehri, H.E. Ali, J.E. Alassafi, A.O.M. Alzahrani, and M.S. Aida, "Al doping influence on the properties of sol–gel synthetized ZnO nanoparticles," Phys. Status Solidi A, **220**, 2300272 (2023). https://doi.org/10.1002/pssa.202300272
[10] M.A. Bouacheria, A. Djelloul, M. Adnane, Y. Larbah, and L. Benharrat, "Characterization of pure and Al doped ZnO thin films prepared by sol gel method for solar cell applications," J. Inorg. Organomet. Polym. Mater. **32**, 2737–2747 (2022). https://doi.org/10.1007/s10904-022-02313-0
[11] M.A. Scarpulla, B. McCandless, A.B. Phillips, Y. Yan, M.J. Heben, C. Wolden, G. Xiong, *et al*., "CdTe-based thin film photovoltaics: Recent advances, current challenges and future prospects," Sol. Energy Mater. Sol. Cells, **255**, 112289 (2023). https://doi.org/10.1016/j.solmat.2023.112289
[12] Y. Tai, J. Li, Y. Zheng, G. Liu, J. Zhang, G. Zeng, K. Yakubov, *et al*., "Research on ultra-thin cadmium telluride heterojunction thin film solar cells," Renew. Sustain. Energy Rev. **207**, 114996 (2025). https://doi.org/10.1016/j.rser.2024.114996
[13] O. Nurmatov, D. Tolaboyev, M. Akhmadjonov, M. Abdubannobov, J. Akhmadaliyev, X. Qodirov, I. Tursunov, and I. Yulchiev, "Role of Deep Defect States in Anomalous Photovoltage Relaxation of Polycrystalline Silver-Doped Cadmium Telluride Thin Films," Informacije MIDEM – Journal of Microelectronics, Electronic Components and Materials, **56**(1), (2026). https://doi.org/10.33180/InfMIDEM2026.105
[14] J. Aranovich, D. Golmayo, A.L. Fahrenbruch, and R.H. Bube, "Photovoltaic properties of ZnO/CdTe heterojunctions prepared by spray pyrolysis," J. Appl. Phys. **51**(8), 4260–4268 (1980). https://doi.org/10.1063/1.328243
[15] J.C. Zepeda Medina, *et al*., "Performance simulation of solar cell based on AZO/CdTe heterostructure by SCAPS 1D software," Heliyon, **9**(3), e14547 (2023). https://doi.org/10.1016/j.heliyon.2023.e14547
[16] J.C. Zepeda Medina, *et al*., "Theoretical improvement of the energy conversion efficiency of an AZO/CdTe heterojunction solar cell to over 27% by incorporating $FeSi_2$ as a second absorber layer," Phys. Scr. **99**, 115987 (2024). https://doi.org/10.1088/1402-4896/ad86fb
[17] F.T. Yusupov, M.F. Akhmadjonov, D.Sh. Khidirov, D.Kh. Tolaboyev, and I.M. Tursunov, "Impact of resistivity on electrical characteristics of Al-doped ZnO/p-Si heterostructures," East Eur. J. Phys. (1), 177–183 (2025). https://doi.org/10.26565/2312-4334-2025-1-17
[18] J.D. Major, "Grain boundaries in CdTe thin film solar cells: A review," Semicond. Sci. Technol. **31**(9), 093001 (2016). https://doi.org/10.1088/0268-1242/31/9/093001
[19] A.I. Zokirov, and B.B. Akhmedov, "Time-controlled synthesis of CdTe quantum dots for tunable photoluminescence," East Eur. J. Phys. (2), 324–329 (2025). https://doi.org/10.26565/2312-4334-2025-2-40
[20] S.K. Cheung, and N.W. Cheung, "Extraction of Schottky diode parameters from forward current-voltage characteristics," Appl. Phys. Lett. **49**(2), 85–87 (1986). https://doi.org/10.1063/1.97359
[21] J. Perrenoud, L. Kranz, S. Buecheler, F. Pianezzi, and A.N. Tiwari, "The use of aluminium doped ZnO as transparent conductive oxide for CdS/CdTe solar cells," Thin Solid Films, **519**(21), 7444–7448 (2011). https://doi.org/10.1016/j.tsf.2010.12.203
[22] L. Kranz, *et al*., "Doping of polycrystalline CdTe for high-efficiency solar cells on flexible metal foil," Nat. Commun. **4**, 2306 (2013). https://doi.org/10.1038/ncomms3306
[23] D. Mora-Herrera, and M. Pal, "Effect of Ge content on diode parameters of superstrate type $Cu_2ZnSn_{1-x}Ge_xS_4$/CdS heterostructures prepared by all-solution process," J. Mater. Sci. **59**, 2416–2436 (2024). https://doi.org/10.1007/s10853-024-09352-7
[24] A. Pandey, S. Dalal, S. Dutta, and A. Dixit, "Structural characterization of polycrystalline thin films by X-ray diffraction techniques," J. Mater. Sci.: Mater. Electron. **32**(2), 1341–1368 (2021). https://doi.org/10.1007/s10854-020-04998-w
[25] P.R. Jubu, O.S. Obaseki, A. Nathan-Abutu, F.K. Yam, Y, Yusof, M.B. Ochang, *et al*., "Dispensability of the conventional Tauc's plot for accurate bandgap determination from UV–Vis optical diffuse reflectance data," Results in Optics, **9**, 100273 (2022). https://doi.org/10.1016/j.rio.2022.100273
[26] P. Scherrer, "Bestimmung der Grösse und der inneren Struktur von Kolloidteilchen mittels Röntgenstrahlen," Nachr. Ges. Wiss. Göttingen, **26**, 98–100 (1918).

ЕКСПЕРИМЕНТАЛЬНА ХАРАКТЕРИСТИКА ТОНКИХ ПЛІВОК ГЕТЕРОПЕРЕХОДУ Al-ЛЕГОВАНОГО ZnO/CdTe, ОТРИМАНИХ МЕТОДОМ SPIN-COATING ІЗ SOL–GEL

Баходір Б. Ахмедов[1], Тохірбек І. Рахмонов[2], Мехріддін Ф. Ахмаджонов[2], Шерзод Ш. Абдуллаєв[2], Іхтійор М. Турсунов[2], Фахріддін Т. Юсупов[2]

[1]Ферганський державний університет, Фергана, Узбекистан
[2]Ферганський державний технічний університет, Фергана, Узбекистан

Оксид цинку, легований l, викликає стійкий інтерес як недорогий, поширений на Землі прозорий провідний оксид n-типу для фотоелектричних систем з гетеропереходами, оброблених розчином. У цій роботі нелеговані тонкі плівки ZnO та AZO (2 мол.% Al/Zn) були нанесені на p-CdTe методом золь-гель спін-покриття та досліджені як прямі гетеропереходи ZnO(AZO)/CdTe без CdS – конфігурація, для якої експериментальні звіти залишаються рідкісними. Структурні, оптичні, електричні та морфологічні реакції були досліджені за допомогою рентгенівської дифракції (XRD), УФ-видимої абсорбційної спектроскопії з аналізом краю зони за першою похідною, темнових та освітлених J-V вимірювань з екстракцією параметрів діода Ченга-Ченга та скануючої електронної мікроскопії (SEM). Рентгенівська дифракція підтвердила співіснування CdTe з цинкової суміші та вюрциту ZnO, орієнтованого з c-осі, з розмірами кристалітів Шеррера 27±5 нм. Максимум похідної абсорбції змістився з 3,31 еВ (ZnO) до 3,33 еВ (AZO). Під впливом освітлення прилад AZO/CdTe показав Jsc ≈ 4,2 мА·см$^{-2}$, Voc ≈ 0,43 В, при n ≈ 3,1, Rs ≈ 28 Ом·см$^{-2}$, Rsh ≈ 310 Ом·см$^{-2}$, FF ≈ 27%, η ≈ 0,49%. СЕМ виявив полікристалічний верхній шар AZO без отворів (зерна 30–80 нм). Результати встановлюють базову характеристику гетеропереходів AZO/CdTe, отриманих шляхом обробки розчином без буфера.

Ключові слова: *Al-легований ZnO; гетероперехід CdTe; золь-гель відцентрове покриття; прозорий провідний оксид; графік Таука; коефіцієнт ідеальності; метод Чунга–Чунга; тонкоплівкова фотовольтаїка*